

Chapter 1

Tight-binding modeling of layered perovskites

1.1 Introduction

After the discovery of the high- T_c superconductors the layered cuprates became one of the most studied materials in solid state physics. A vast range of compounds were synthesised and their properties comprehensively investigated. The electron band structure is of particular importance for understanding the nature of superconductivity in this type of perovskites [9]. Along this line one can single out the significant success achieved in the attempts to reconcile the photoelectron spectroscopy data [10, 11] and the band structure calculations of the Fermi surface (FS) especially for compounds with simple structure such as $\text{Nd}_{2-x}\text{Ce}_x\text{CuO}_{4-\delta}$ [12, 13]. A qualitative understanding, at least for the self-consistent electron picture, has been achieved and for the most electron processes in the layered perovskites one can employ adequate lattice models.

At the time when we actually started working on the subject of this book, there was not much analysis of the electronic band structures of the high- T_c materials in the terms of single analytical expressions available. This is something for which there was a clear need, in particular to help in the construction of more realistic many-body Hamiltonians. The aim of this chapter is to analyse the common features in the electron band structure of the layered perovskites within the tight-binding (TB) method (for a nice review see references [14–16]). In the following we shall focus on the metallic (being eventually superconducting) phase only, with the provision that the antiferromagnetic correlations, especially in the dielectric phase, could substantially alter the electron dispersion. It is shown that the linear combination of atomic orbitals (LCAO) approximation can be considered as an adequate tool for analysis of energy

bands. Within the latter exact analytic results are obtained for the constant energy contours (CEC). These expressions are used to fit the FS of $\text{Nd}_{2-x}\text{Ce}_x\text{CuO}_{4-\delta}$ [12], $\text{Pb}_{0.42}\text{Bi}_{1.73}\text{Sr}_{1.94}\text{Ca}_{1.3}\text{Cu}_{1.92}\text{O}_{8+x}$ [17–21], and Sr_2RuO_4 [22] mapped in angle-resolved photoemission/angle-resolved ultraviolet spectroscopy (ARPES/ARUPS) experiments.

To address the conduction bands in the layered perovskites we start from a common Hamiltonian including the basis of valence states $\text{O}2p$, and $\text{Ru}4d\varepsilon$, or $\text{Cu}3d_{x^2-y^2}$, $\text{Cu}4s$, for ruthenates and cuprates, respectively. Despite the equivalent crystal structure of Sr_2RuO_4 [23] and $\text{La}_{2-x}\text{Ba}_x\text{CuO}_4$ [1, 24], the states in their conduction band(s) are, in some sense, complementary. In other words, for the CuO_2 plane the conduction band is of σ -character while for the RuO_2 plane the conduction bands are determined by π valence bonds. This is due to the separation into σ - and π -part of the Hamiltonian $H = H^{(\sigma)} + H^{(\pi)}$ in first approximation. The latter two Hamiltonians are studied separately.

This chapter is organized as follows. After a few remarks on the applicability of the TB model and a brief apology to the band theory in general, in Sec. 1.3 we consider the generic $H^{(4\sigma)}$ Hamiltonian of the CuO_2 plane [25–27] and $H^{(\pi)} = H^{(xy)} + H^{(z)}$ is then studied in Sec. 1.4. The results of the comparison with the experimental data are summarised in Sec. 1.5 and the last section discusses practical aspects in connecting the present theory with experiment.

1.2 Apology to the band theory

It is well-known that the electron band theory is a self-consistent treatment of the electron motion in the crystal lattice. Even the classical 3-body problem demonstrates strongly correlated solutions, so it is *a priori* unknown whether the self-consistent approximation is applicable when describing the electronic structure of every new crystal. However, the one-particle band picture is an indispensable stage in the complex study of materials. It is the analysis of experimental data using a conceptually clear band theory that reveals nontrivial effects: how strong the strongly correlated electronic effects are, whether it is possible to take into account the influence of some interaction-induced order parameter back into the electronic structure etc. Therefore the comparison of the experiment with the band calculations is not an attempt, as sometimes thought, to hide the relevant issues—it is a tool to reveal interesting and nontrivial properties of the electronic structure.

Many electron band calculations have been performed for the layered perovskites and results were compared to data due to ARPES experiments. The shape of the Fermi surface is probably the simplest test to check whether we are on the right track or some conceptually new theory should be used from the very beginning.

The tight-binding interpolation of the electronic structure is often used for fitting the experimental data. This is because the accuracy of that approximation is often higher than the uncertainties in the experiment. Moreover, the tight-binding method gives simple formulae which could be of use for experimentalists to see how far they can get with such a simple minded approach. The tight-binding parameters, however, have in a sense “their own life” independent of the *ab initio* calculations. These parameters can be fitted directly to the experiment even when, by some reasons, the electron band calculations could give wrong predictions. In this sense the tight-binding parameters are the appropriate intermediary between the theory and experiment. As for the theory, establishing of reliable one-particle tight-binding parameters is the preliminary step in constructing more realistic many-body Hamiltonians. The role of the band theory is, thus, quite ambivalent: on one hand, it is the final “language” used in efforts towards understanding a broad variety of phenomena; on the other hand, it is the starting point in developing realistic interaction Hamiltonians for sophisticated phenomena such as magnetism and superconductivity.

The tight-binding method is the simplest one employed in the electron band calculations and it is described in every textbook in solid state physics; the layered perovskites are now probably the best investigated materials [2, 28, 29] and the Fermi surface is a fundamental notion in the physics of metals. There is a consensus that the superconductivity of layered perovskites is related to electron processes in the CuO_2 and RuO_2 planes of these materials. It is not, however, fair to criticise a given study, employing the tight-binding method as an interpolation scheme to the first principles calculations, for not thoroughly discussing the many-body effects. The criticism should rather be redirected to the *ab initio* electronic structure calculations. An interpolation scheme cannot contain more information than the underlying theory. It is not erroneous if such a scheme works with an accuracy high enough to adequately describe both the theory and experiment.

In view of the above, we found it strange that there were no simple interpolation formulae for the Fermi surfaces available in the literature and the experimental data were being published without an attempt towards

simple interpretation. One of the aims of the present chapter was initially to help interpret the experimental data by the tight-binding method as well as setting up notions for the analysis of the *ab initio* calculations.

1.3 Layered cuprates

The CuO₂ plane appears as a common structural detail for all layered cuprates. Therefore, in order to retain the generality of the considerations, the electronic properties of the bare CuO₂ plane will be addressed without taking into account structural details such as dimpling, orthorhombic distortion, double planes, surrounding chains etc. For the square unit cell with lattice constant a_0 three-atomic basis is assumed $\{\mathbf{R}_{\text{Cu}}, \mathbf{R}_{\text{O}_a}, \mathbf{R}_{\text{O}_b}\} = \{\mathbf{0}, (a_0/2, 0), (0, a_0/2)\}$. The unit cell is indexed by vector $\mathbf{n} = (n_x, n_y)$, where $n_x, n_y = \text{integer}$. Within such an idealized model the LCAO wave function spanned over the $|\text{Cu}3d_{x^2-y^2}\rangle, |\text{Cu}4s\rangle, |\text{O}_a2p_x\rangle, |\text{O}_b2p_y\rangle$ states reads

$$\begin{aligned} \psi_{\text{LCAO}}(\mathbf{r}) = \sum_{\mathbf{n}} \bigg[& X_{\mathbf{n}} \psi_{\text{O}_a2p_x}(\mathbf{r} - \mathbf{R}_{\text{O}_a} - a_0\mathbf{n}) \\ & + Y_{\mathbf{n}} \psi_{\text{O}_b2p_y}(\mathbf{r} - \mathbf{R}_{\text{O}_b} - a_0\mathbf{n}) + S_{\mathbf{n}} \psi_{\text{Cu}4s}(\mathbf{r} - \mathbf{R}_{\text{Cu}} - a_0\mathbf{n}) \\ & + D_{\mathbf{n}} \psi_{\text{Cu}3d_{x^2-y^2}}(\mathbf{r} - \mathbf{R}_{\text{Cu}} - a_0\mathbf{n}) \bigg], \end{aligned} \quad (1.1)$$

where $\Psi_{\mathbf{n}} = (D_{\mathbf{n}}, S_{\mathbf{n}}, X_{\mathbf{n}}, Y_{\mathbf{n}})$ is the tight-binding wave function in lattice representation.

The neglect of the differential overlap leads to an LCAO Hamiltonian of the CuO₂ plane

$$\begin{aligned} H = \sum_{\mathbf{n}} \bigg\{ & D_{\mathbf{n}}^\dagger [-t_{pd}(-X_{\mathbf{n}} + X_{x-1,y} + Y_{\mathbf{n}} - Y_{x,y-1}) + \epsilon_d D_{\mathbf{n}}] \\ & + S_{\mathbf{n}}^\dagger [-t_{sp}(-X_{\mathbf{n}} + X_{x-1,y} - Y_{\mathbf{n}} + Y_{x,y-1}) + \epsilon_s S_{\mathbf{n}}] \\ & + X_{\mathbf{n}}^\dagger [-t_{pp}(Y_{\mathbf{n}} - Y_{x+1,y} - Y_{x,y-1} + Y_{x+1,y-1}) \\ & \quad - t_{sp}(-S_{\mathbf{n}} + S_{x+1,y}) - t_{pd}(-D_{\mathbf{n}} + D_{x+1,y}) + \epsilon_p X_{\mathbf{n}}] \\ & + Y_{\mathbf{n}}^\dagger [-t_{pp}(X_{\mathbf{n}} - X_{x-1,y} - X_{x,y+1} + X_{x-1,y+1}) \\ & \quad - t_{sp}(-S_{\mathbf{n}} + S_{x,y+1}) - t_{pd}(D_{\mathbf{n}} + D_{x,y+1}) + \epsilon_p Y_{\mathbf{n}}] \bigg\}, \end{aligned} \quad (1.2)$$

where the components of $\Psi_{\mathbf{n}}$ should be considered as being Fermi operators. The notations ϵ_d, ϵ_s , and ϵ_p stand respectively for the Cu3d_{x²-y²}, Cu4s and O2p σ single-site energies. The direct O_a2p_x \rightarrow O_b2p_y exchange is denoted by t_{pp} and similarly t_{sp} and t_{pd} denote the Cu4s \rightarrow O2p and O2p \rightarrow

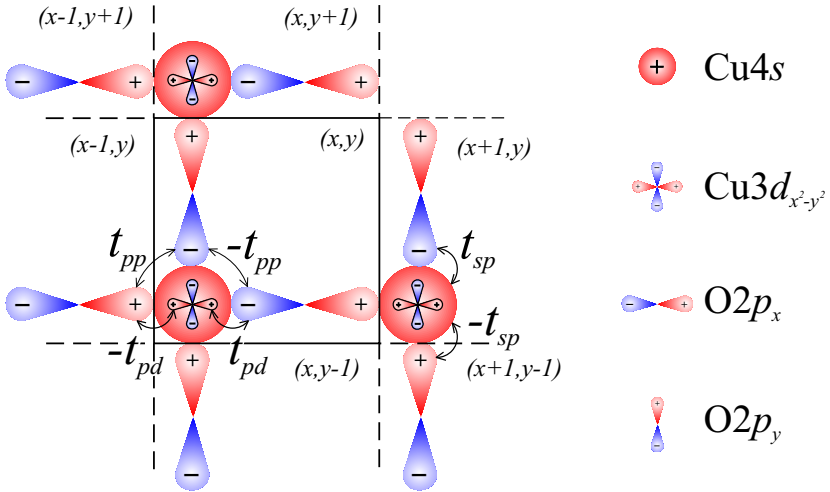


Fig. 1.1 Schematic of a CuO₂ plane (only orbitals relevant to the discussion are depicted). The solid square represents the unit cell with respect to which the positions of the other cells are determined. The indices of the wave function amplitudes involved in the LCAO Hamiltonian (1.2) are given in brackets. The rules for determining the signs of hopping integrals t_{pd} , t_{sp} , and t_{pp} are shown as well.

Cu3d_{x²-y²} hoppings respectively. The sign rules for the hopping amplitudes are sketched in Fig. 1.1 — the bonding orbitals enter the Hamiltonian with a negative sign.

For the Bloch states diagonalizing the Hamiltonian (1.2)

$$\Psi_{\mathbf{n}} \equiv \begin{pmatrix} D_{\mathbf{n}} \\ S_{\mathbf{n}} \\ X_{\mathbf{n}} \\ Y_{\mathbf{n}} \end{pmatrix} = \frac{1}{\sqrt{N}} \sum_{\mathbf{p}} \begin{pmatrix} D_{\mathbf{p}} \\ S_{\mathbf{p}} \\ e^{i\varphi_a} X_{\mathbf{p}} \\ e^{i\varphi_b} Y_{\mathbf{p}} \end{pmatrix} e^{i\mathbf{p}\cdot\mathbf{n}}, \quad (1.3)$$

where N is the number of unit cells, we use the same phases as in references [25–27]:

$$\varphi_a = \frac{1}{2}(p_x - \pi), \quad \varphi_b = \frac{1}{2}(p_y - \pi). \quad (1.4)$$

Equation (1.3) describes the Fourier transform between the coordinate representation $\Psi_{\mathbf{n}} = (D_{\mathbf{n}}, S_{\mathbf{n}}, X_{\mathbf{n}}, Y_{\mathbf{n}})$, with \mathbf{n} being the cell index, and the momentum representation $\psi_{\mathbf{p}} = (D_{\mathbf{p}}, S_{\mathbf{p}}, X_{\mathbf{p}}, Y_{\mathbf{p}})$ of the TB wave function (when used as an index, the electron quasi-momentum vector is denoted by p). Hence, the Schrödinger equation $i\hbar d_t \hat{\psi}_{p,\alpha} = [\hat{\psi}_{p,\alpha}, \hat{H}]$ for

$\psi_{p,\alpha}(t) = e^{-i\epsilon t/\hbar}\psi_{p,\alpha}$, with α being the spin index (\uparrow, \downarrow) (suppressed hereafter) and ϵ the band energy, takes the form

$$\left(H_p^{(4\sigma)} - \epsilon \mathbf{1}\right) \psi_p = \begin{pmatrix} -\epsilon_d & 0 & t_{pd}s_x & -t_{pd}s_y \\ 0 & -\epsilon_s & t_{sp}s_x & t_{sp}s_y \\ t_{pd}s_x & t_{sp}s_x & -\epsilon_p & -t_{pp}s_x s_y \\ -t_{pd}s_y & t_{sp}s_y & -t_{pp}s_x s_y & -\epsilon_p \end{pmatrix} \begin{pmatrix} D_p \\ S_p \\ X_p \\ Y_p \end{pmatrix} = 0, \quad (1.5)$$

where

$$\epsilon_d = \epsilon - \epsilon_d, \quad \epsilon_s = \epsilon - \epsilon_s, \quad \epsilon_p = \epsilon - \epsilon_p, \quad (1.6)$$

and

$$\begin{aligned} s_x &= 2 \sin\left(\frac{1}{2}p_x\right) & x &= \sin^2\left(\frac{1}{2}p_x\right) \\ s_y &= 2 \sin\left(\frac{1}{2}p_y\right) & y &= \sin^2\left(\frac{1}{2}p_y\right) \\ 0 &\leq p_x, p_y \leq 2\pi. \end{aligned} \quad (1.7)$$

This 4σ -band Hamiltonian is generic for the layered cuprates, cf. Ref. [27]. We have also included the direct oxygen-oxygen exchange t_{pp} dominated by the σ amplitude. The secular equation

$$\det\left(H_p^{(4\sigma)} - \epsilon \mathbf{1}\right) = \mathcal{A}xy + \mathcal{B}(x + y) + \mathcal{C} = 0 \quad (1.8)$$

gives the spectrum and the canonical form of the CEC with energy-dependent coefficients

$$\begin{aligned} \mathcal{A}(\epsilon) &= 16(4t_{pd}^2 t_{sp}^2 + 2t_{sp}^2 t_{pp}\epsilon_d - 2t_{pd}^2 t_{pp}\epsilon_s - t_{pp}^2 \epsilon_d \epsilon_s) \\ \mathcal{B}(\epsilon) &= -4\epsilon_p(t_{sp}^2 \epsilon_d + t_{pd}^2 \epsilon_s) \\ \mathcal{C}(\epsilon) &= \epsilon_d \epsilon_s \epsilon_p^2. \end{aligned} \quad (1.9)$$

Hence, the explicit CEC equation reads as

$$p_y = \pm 2 \arcsin \sqrt{y}, \quad \text{if } 0 \leq y = -\frac{\mathcal{B}x + \mathcal{C}}{\mathcal{A}x + \mathcal{B}} \leq 1. \quad (1.10)$$

This equation reproduces the rounded square-shaped Fermi surface, centered at the (π, π) point, inherent for all layered cuprates. The best fit is achieved when \mathcal{A} , \mathcal{B} and \mathcal{C} are considered as fitting parameters. Thus, for a CEC passing through the D = (p_d, p_d) and C = (p_c, π) reference points, as indicated in Fig. 1.2, the fitting coefficients (distinguished by the subscript f) in the canonical equation

$$\mathcal{A}_f xy + \mathcal{B}_f(x + y) + \mathcal{C}_f = 0 \quad (1.11)$$

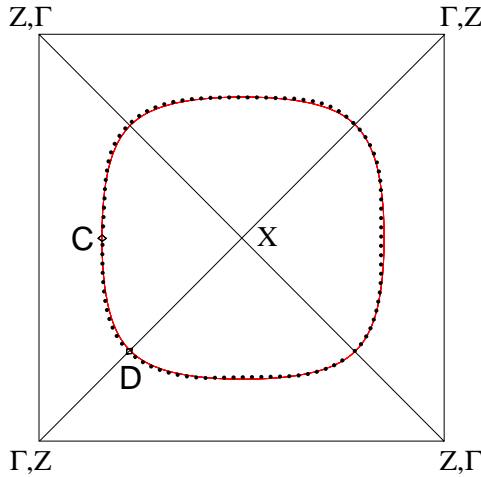


Fig. 1.2 LDA Fermi contour of $\text{Nd}_{2-x}\text{Ce}_x\text{CuO}_{4-\delta}$ (dotted line) calculated by Yu and Freeman [13] (courtesy of the authors), and the LCAO fit (solid line) according to Eq. (1.8). The fitting procedure uses C and D as reference points.

have the form

$$\begin{aligned}
 \mathcal{A}_f &= 2x_d - x_c - 1, & x_d &= \sin^2(p_d/2) \\
 \mathcal{B}_f &= x_c - x_d^2, & x_c &= \sin^2(p_c/2) \\
 \mathcal{C}_f &= x_d^2(x_c + 1) - 2x_c x_d,
 \end{aligned} \tag{1.12}$$

and the resulting LCAO Fermi contour is quite compatible with the local-density approximation (LDA) calculations for $\text{Nd}_{2-x}\text{Ce}_x\text{CuO}_{4-\delta}$ [13, 30]. Due to the simple shape of the FS the curves just coincide. We note also that the canonical equation (1.8) would formally correspond to 1-band TB Hamiltonian of a 2D square lattice of the form

$$\epsilon(\mathbf{p}) = -2t(\cos p_x + \cos p_y) + 4t' \cos p_x \cos p_y,$$

with strong energy dependence of the hopping parameters, where t' is the anti-bonding hopping between the sites along the diagonal, cf. [31–33].

1.3.1 Effective Cu Hamiltonian

Studies of the electronic structure of the layered cuprates have unambiguously proved the existence of a large hole pocket — a rounded square centred at the (π, π) point. This observation is indicative for a Fermi level located in a single band of dominant $\text{Cu}3d_{x^2-y^2}$ character. To address this band

and the related wave functions, it is therefore convenient for an effective Cu-Hamiltonian to be derived by Löwdin downfolding of the oxygen orbitals. This is equivalent to expressing the oxygen amplitudes from the third and fourth rows of Eq. (1.5)

$$\begin{aligned} X &= \frac{1}{\eta_p} \left[t_{pd}s_x \left(1 + \frac{t_{pp}}{\varepsilon_p} s_y^2 \right) D + t_{sp}s_x \left(1 - \frac{t_{pp}}{\varepsilon_p} s_y^2 \right) S \right] \\ Y &= \frac{1}{\eta_p} \left[-t_{pd}s_y \left(1 + \frac{t_{pp}}{\varepsilon_p} s_x^2 \right) D + t_{sp}s_y \left(1 - \frac{t_{pp}}{\varepsilon_p} s_x^2 \right) S \right], \end{aligned} \quad (1.13)$$

where $\eta_p = \varepsilon_p - \frac{t_{pp}^2}{\varepsilon_p} s_x^2 s_y^2$, and substituting back into the first and the second rows of the same equation. Such a downfolding procedure results in the following energy-dependent copper Hamiltonian

$$H_{Cu}(\epsilon) = \begin{pmatrix} \epsilon_d + \frac{(2t_{pd})^2}{\eta_p} \left(x + y + \frac{8t_{pp}}{\varepsilon_p} xy \right) & \frac{(2t_{pd})(2t_{sp})}{\eta_p} (x - y) \\ \frac{(2t_{pd})(2t_{sp})}{\eta_p} (x - y) & \epsilon_s + \frac{(2t_{pd})^2}{\eta_p} \left(x + y - \frac{8t_{pp}}{\varepsilon_p} xy \right) \end{pmatrix}, \quad (1.14)$$

which enters the effective Schrödinger equation $H_{Cu} \begin{pmatrix} D \\ S \end{pmatrix} = \epsilon \begin{pmatrix} D \\ S \end{pmatrix}$. Thus, from Eq. (1.13) and Eq. (1.14) one can easily obtain an approximate expression for the eigenvector corresponding to a dominant $Cu3d_{x^2-y^2}$ character. Taking $D \approx 1$, in the lowest order with respect to the hopping amplitudes t_{ij} one has

$$|Cu3d_{x^2-y^2}\rangle = \begin{pmatrix} D \\ S \\ X \\ Y \end{pmatrix} \approx \begin{pmatrix} 1 \\ (t_{sp}t_{pd}/\varepsilon_s\varepsilon_p)(s_x^2 - s_y^2) \\ (t_{pd}/\eta_p)s_x \\ -(t_{pd}/\eta_p)s_y \end{pmatrix}, \quad (1.15)$$

i.e., $|X|^2 + |Y|^2 + |S|^2 \ll |D|^2 \approx 1$. We note that within this Cu scenario the Fermi level location and the CEC shape are not sensitive to t_{pp} . Therefore one can neglect the oxygen-oxygen hopping as was done, for example, by Andersen *et al.* [25–27] (the importance of the t_{pp} parameter has been considered by Markiewicz [34]) and the band structure of the Hamiltonian (1.14) for the same set of energy parameters as used in Ref. [27] is shown in Fig. 1.3 (a). In this case, the Fermi surface can be fitted by its diagonal alone, i.e., using D alone as a reference point. Hence an equation for the Fermi energy follows, $\mathcal{A}(\epsilon_F)x_d^2 + 2\mathcal{B}(\epsilon_F)x_d + \mathcal{C}(\epsilon_F) = 0$, which yields $\epsilon_F = 2.5$ eV. As seen in Fig. 1.3 (b), the deviation from the two-parameter fit is almost vanishing, thus justifying the neglect of t_{pp}

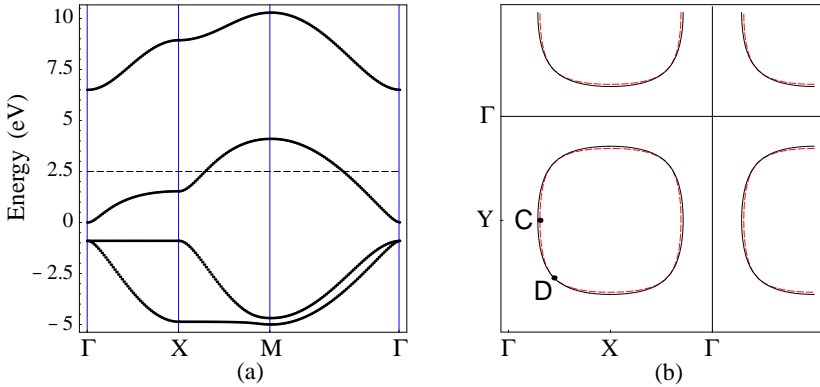


Fig. 1.3 (a) Electron band structure of the generic for the CuO_2 plane 4σ -band Hamiltonian using the parameters from Ref. [27] and the Fermi level $\epsilon_F = 2.5$ eV fitted from the LDA calculation by Yu and Freeman [13]; (b) The LCAO Fermi contour (solid line) fitted to the LDA Fermi surface (dashed line) for $\text{Nd}_{2-x}\text{Ce}_x\text{CuO}_{4-\delta}$ [13] using only D as a reference point. The deviation of the fit at the C point is negligible.

and using the one-parameter fit. However, despite the excellent agreement between the LDA calculations, the LCAO fit and the ARPES data regarding the FS shape, the theoretically calculated conduction bandwidth w_c in the layered cuprates is overestimated by a factor of 2 or even 3 [12]. Equation (1.11) describes acceptably also the experimental ARPES data, e.g., for $\text{Nd}_{2-x}\text{Ce}_x\text{CuO}_{4-\delta}$, material with single CuO_2 plane and no other complicating structural details. In Fig. 1.4 we compare the ARPES data from Ref. [12] and the Fermi contour calculated for $x = 0.15$.

There exist a tremendous number of ARPES/ARUPS data for layered cuprates which makes the reviewing of all those spectra impossible. To further illustrate our TB model we have chosen the data for Pb substitution for Bi in $\text{Bi}_2\text{Sr}_2\text{CaCu}_2\text{O}_8$. The ARUPS Fermi surface of $\text{Pb}_{0.42}\text{Bi}_{1.73}\text{Sr}_{1.94}\text{Ca}_{1.3}\text{Cu}_{1.92}\text{O}_{8+x}$ [17–21] is shown in Fig. 1.5 (a). In this case the CuO_2 planes are quite flat and the ARPES data are not distorted by structural details. When present, distortions were eventually misinterpreted as a manifestation of strong antiferromagnetic correlations. We believe, however, that the experiment by Schwaller *et al.* [21] reveals the main feature of the CuO_2 plane band structure — the large hole pocket found to be in agreement with the one-particle band calculations. Strong support to this view comes from a paper by Campuzano *et al.* [35] where the ARPES Fermi surface of pure $\text{Bi}_2\text{Sr}_2\text{CaCu}_2\text{O}_{8+\delta}$ was mapped [cf. the inset of Fig. 1 (a) therein]. This experimental finding is

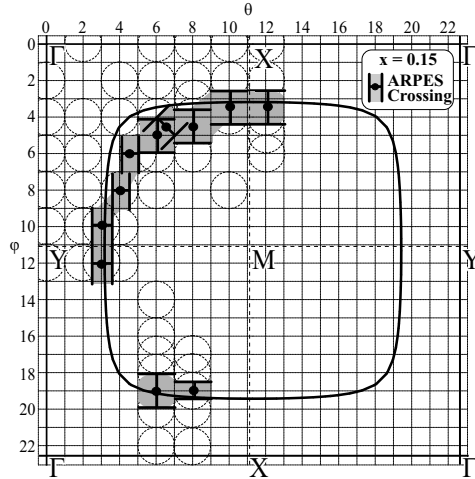


Fig. 1.4 The Fermi surface of $\text{Nd}_{2-x}\text{Ce}_x\text{CuO}_{4-\delta}$ (solid line) determined by equation Eq. (1.11) for $x = 0.15$ and compared with experimental data (points with error bars) for the same value of x after King *et al.* [12]. θ and φ denote the polar and azimuthal emission angles, respectively, measured in degrees. The empty dashed circles show \mathbf{k} -space locations where ARPES experiments have been performed (cf. Fig. 2 in Ref. [12]) and their diameter corresponds to 2° experimental resolution.

in excellent agreement with our tight-binding fit to the Fermi surface of $\text{Pb}_{0.42}\text{Bi}_{1.73}\text{Sr}_{1.94}\text{Ca}_{1.3}\text{Cu}_{1.92}\text{O}_{8+x}$, studied by Schwaller and co-workers in Ref. [21], Fig. 1.5 (b). The remarkable coincidence of the Fermi surfaces of these two compounds is a nice confirmation that Pb substitution for Bi is irrelevant for the band structure of the CuO_2 plane and the Fermi surface of the latter is therefore revealed to be a common feature.

1.4 Conduction bands of the RuO_2 plane

Sr_2RuO_4 is the first copper-free perovskite superconductor isostructural to the high- T_c cuprates [23]. The layered ruthenates, just like the layered cuprates, are strongly anisotropic and in first approximation the nature of the conduction band(s) can be understood by analysing the bare RuO_2 plane. One should repeat the same steps as in the previous section but now having Ru instead of Cu and the Fermi level located in the metallic bands of $\text{Ru}4d\pi$ character. To be specific, the conduction bands arise from the hybridisation between the $\text{Ru}4d_{xy}$, $\text{Ru}4d_{yz}$, $\text{Ru}4d_{zx}$ and O_a2p_y , O_b2p_x , $O_{a,b}2p_z$ π -orbitals. The LCAO wave function spanned over the four

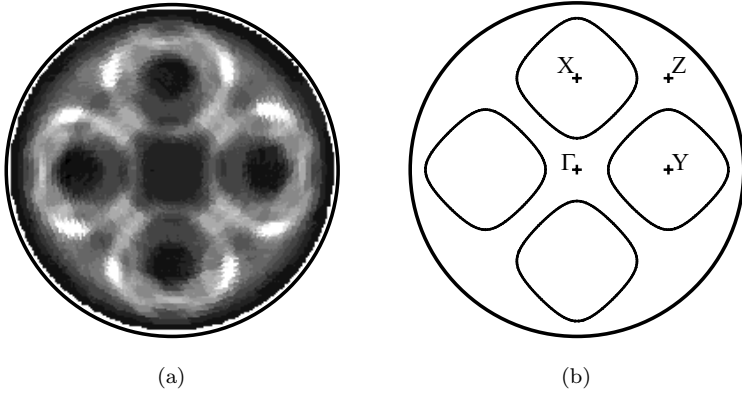


Fig. 1.5 (a) ARUPS Fermi surface of $\text{Pb}_{0.42}\text{Bi}_{1.73}\text{Sr}_{1.94}\text{Ca}_{1.3}\text{Cu}_{1.92}\text{O}_{8+x}$ by Schwaller *et al.* [21]; (b) LCAO fit to (a) according to Eq. (1.11) using the D reference point with $p_d = 0.171 \times 2\pi$.

perpendicular to the RuO_2 plane orbitals reads

$$\begin{aligned} \Psi_{\text{LCAO}}^{(z)}(\mathbf{r}) = & \frac{1}{\sqrt{N}} \sum_{\mathbf{p}} \sum_{\mathbf{n}} \left[D_{zx,\mathbf{n}} \psi_{\text{Ru}4d_{zx}}(\mathbf{r} - a_0\mathbf{n}) \right. \\ & + D_{zy,\mathbf{n}} \psi_{\text{Ru}4d_{zy}}(\mathbf{r} - a_0\mathbf{n}) + e^{i\varphi_a} Z_{a,\mathbf{n}} \psi_{\text{O}_a2p_z}(\mathbf{r} - \mathbf{R}_{\text{O}_a} - a_0\mathbf{n}) \\ & \left. + e^{i\varphi_b} Z_{b,\mathbf{n}} \psi_{\text{O}_b2p_z}(\mathbf{r} - \mathbf{R}_{\text{O}_b} - a_0\mathbf{n}) \right] e^{i\mathbf{p}\cdot\mathbf{n}} \end{aligned} \quad (1.16)$$

Hence, the π -analog of Eq. (1.5) takes the form

$$\left(H_p^{(z)} - \epsilon \mathbf{1} \right) \psi_p^{(z)} = \begin{pmatrix} -\epsilon_{zx} & 0 & t_{z,zx}s_x & 0 \\ 0 & -\epsilon_{zy} & 0 & t_{z,zy}s_y \\ t_{z,zx}s_x & 0 & -\epsilon_{za} & -t_{zz}c_x c_y \\ 0 & t_{z,zy}s_y & -t_{zz}c_x c_y & -\epsilon_{zb} \end{pmatrix} \begin{pmatrix} D_{zx} \\ D_{zy} \\ Z_a \\ Z_b \end{pmatrix} = 0, \quad (1.17)$$

where

$$\begin{aligned} \epsilon_{zx} &= \epsilon - \epsilon_{zx}, & \epsilon_{za} &= \epsilon - \epsilon_{za}, & c_x &= 2 \cos(p_x/2), \\ \epsilon_{zy} &= \epsilon - \epsilon_{zy}, & \epsilon_{zb} &= \epsilon - \epsilon_{zb}, & c_y &= 2 \cos(p_y/2), \end{aligned} \quad (1.18)$$

and ϵ_{zx} , ϵ_{zy} , ϵ_{za} , and ϵ_{zb} are the single site energies of the $\text{Ru}4d_{zx}$, $\text{Ru}4d_{zy}$ and O_a2p_z , O_b2p_z orbitals, respectively. t_{zz} denotes the hopping between the latter two orbitals and, assuming a negligible orthorhombic distortion, the metal-oxygen π -hopping parameters are equal, $t_{z,zy} = t_{z,zx}$ and also $\epsilon_z = \epsilon_{za} = \epsilon_{zb}$. The phase factors $e^{i\varphi_{a,b}}$ in Eq. (1.16) are chosen in compliance with Ref. [27], see Eq. (1.4).

Similarly, writing the LCAO wave function spanned over the three in-plane π -orbitals $\text{Ru}4d_{xy}$, O_a2p_y , and O_b2p_x in the way in which Eq. (1.16) is designed one has for the “in-plane” Schrödinger equation

$$\left(H_p^{(xy)} - \epsilon \mathbf{1}\right) \psi_p^{(xy)} = \begin{pmatrix} -\epsilon_{xy} & t_{pd\pi} s_x & t_{pd\pi} s_y \\ t_{pd\pi} s_x & -\epsilon_{ya} & t'_{pp} s_x s_y \\ t_{pd\pi} s_y & t'_{pp} s_x s_y & -\epsilon_{xb} \end{pmatrix} \begin{pmatrix} D_{xy} \\ Y_a \\ X_b \end{pmatrix} = 0, \quad (1.19)$$

where $t_{pd\pi}$ and t'_{pp} denote the $\text{Ru}4d_{xy} \rightarrow \text{O}_{a,b}2p\pi$ and $\text{O}_a2p_y \rightarrow \text{O}_b2p_x$ hoppings, respectively. The definitions for the other energy parameters are in analogy to Eq. (1.18) (for negligible orthorhombic distortion $\epsilon_{ya} = \epsilon_{xb} \neq \epsilon_z$). Thus, the π -Hamiltonian of the RuO_2 plane takes the form

$$H^{(\pi)} = \sum_{p,\alpha=\uparrow,\downarrow} \psi_{p,\alpha}^{(z)\dagger} H_p^{(z)} \psi_{p,\alpha}^{(z)} + \psi_{p,\alpha}^{(xy)\dagger} H_p^{(xy)} \psi_{p,\alpha}^{(xy)}. \quad (1.20)$$

The derivation of the corresponding secular equations was announced in a couple of short publications [36,37]. Here we shall only provide the final expressions in terms of the notation used here

$$\begin{aligned} \det(H_p^{(z,xy)} - \epsilon \mathbf{1}) &= \mathcal{A}^{(z,xy)} xy + \mathcal{B}^{(z,xy)} (x + y) + \mathcal{C}^{(z,xy)} = 0, \\ \mathcal{A}^{(z)} &= 16(t_{z,zx}^4 - t_{zz}^2 \epsilon_{zx}^2) & \mathcal{A}^{(xy)} &= 32t'_{pp} t_{pd\pi}^2 - 16\epsilon_{xy} t_{pp}^2 \\ \mathcal{B}^{(z)} &= -16t_{zz}^2 \epsilon_{zx}^2 - 4t_{z,zx}^2 \epsilon_{zx} \epsilon_z & \mathcal{B}^{(xy)} &= -t_{pd\pi}^2 \epsilon_{ya} \\ \mathcal{C}^{(z)} &= \epsilon_{zx}^2 (\epsilon_z^2 - 16t_{zz}^2) & \mathcal{C}^{(xy)} &= \epsilon_{xy} \epsilon_{ya}. \end{aligned} \quad (1.21)$$

The three sheets of the Fermi surface in Sr_2RuO_4 fitted to the ARPES data by Lu *et al.* [22] are shown in Fig. 1.6 (b). To determine the Hamiltonian parameters we have made use of the eigenvalues at the high-symmetry points of the Brillouin zone. To the best of our knowledge, the TB analysis of the Sr_2RuO_4 band structure was first performed in Refs. [36,37]. Subsequently, the latter results were reproduced in Ref. [38] without referring to Refs. [36,37]. The RuO_2 -plane band structure resulting from the set of parameters

$$\begin{aligned} t_{zz} &= t'_{pp} = 0.3 \text{ eV} & \epsilon_z &= -2.3 \text{ eV} & \epsilon_{xy} &= -1.62 \text{ eV} \\ t_{pd\pi} &= t_{z,zx} = 1 \text{ eV} & \epsilon_{zx} &= -1.3 \text{ eV} & \epsilon_{ya,xb} &= -2.62 \text{ eV} \end{aligned} \quad (1.22)$$

is shown in Fig. 1.6 (a). This fit is subjected to the requirement of providing as good as possible a description of the narrow energy window around ϵ_F whereas the filled bands, far below the Fermi level, might only qualitatively match the LDA calculations by Oguchi [39] and Singh [40]. Furthermore, the Sr_2RuO_4 Fermi surface mapping, based on the de Haas–van Alphen

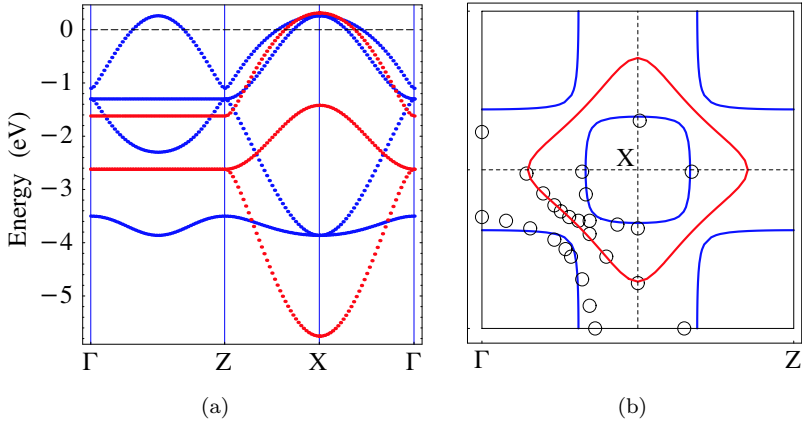


Fig. 1.6 (a) LCAO band structure of Sr_2RuO_4 according to Eq. (1.20). The Fermi level (dashed line) crosses the three $\text{Ru}4d\varepsilon$ bands of the RuO_2 plane; (b) LCAO fit (solid lines) to the ARPES data (circles) by Lu *et al.* [22], cf. also Ref. [36,37].

(dHvA) effect [41], differs from the ARPES results [22]. Thus, fitting the dHvA data by using modified TB parameters is a natural refinement of the proposed model. We note that the diamond-shaped hole pocket, centred at the X point, Fig. 1.6 (b), is very sensitive to the “game of parameters”. For that band the van Hove energy is fairly close to the Fermi energy. As a result, a minor change in the parameters could drive a van Hove transition transforming this hole pocket into an electron one, centred at the Γ point. Indeed, such a band arrangement has also been observed in the ARPES revision of the Sr_2RuO_4 Fermi surface [42] and reflects the topology of the energy surfaces $\epsilon(\mathbf{p})$ derived in Refs. [36,37]. The comparison of the ARPES data with TB energy surfaces could be the subject of a separate study.

1.5 Discussion

The LCAO analysis of the layered perovskites band structure, performed in the preceding sections, manifests a good compatibility with the experimental data and the band calculations as well. Due to the strong anisotropy of these materials, their FS within a reasonable approximation is determined by the properties of the bare CuO_2 or RuO_2 planes.

Despite these planes having identical crystal structure, their electronic structures are quite different. While for the RuO_2 plane the Fermi level crosses metallic π -bands, the conduction band of the CuO_2 plane

is described by a σ -Hamiltonian (1.5). The latter gives for the CuO_2 plane a large hole pocket centered at the (π, π) point. Its shape, if no additional sheets exist, is well-described by the exact analytic results within the LCAO model, Eq. (1.8), as found for $\text{Nd}_{2-x}\text{Ce}_x\text{CuO}_{4-\delta}$ [12, 13] and $\text{Pb}_{0.42}\text{Bi}_{1.73}\text{Sr}_{1.94}\text{Ca}_{1.3}\text{Cu}_{1.92}\text{O}_{8+x}$ [17–21]. For a number of other cuprates,¹ this large hole pocket is easily identified. For all of the above compounds, however, its shape is usually deformed due to appearance of additional sheets of the Fermi surface originating from accessories of the crystal structure.

The applicability of the LCAO approximation to the electronic structure of the layered cuprates can be considered as being proved. The basis functions of the LCAO Hamiltonian can be included in a realistic one-electron part of the lattice Hamiltonians for the layered perovskites. This is an indispensable step preceding the inclusion of the two electron exchange (Chapter 2), electron-phonon interaction or any other interactions between conducting electrons.

1.6 Determining the density of states of thin high- T_c films by field-effect-transistor type microstructures

The importance of the density of states (DOS) for the physics of high- T_c cuprates has been discussed in many papers [34, 54–62]. In this section we shall suggest a simple electronic method for determining the DOS. The proposed experiment requires (i) preparation of a field-effect transistor (FET) type microstructure and (ii) standard electronic measurement. The FET controls the current between two points but does so differently than the bipolar transistor. The FET relies on an electric field to control the shape and hence the conductivity of a “channel” in a semiconductor material. The shape of the conducting channel in a FET is altered when a potential difference is applied to the gate terminal (potential relative to either source or drain). It causes the electrons flow to change its width and thus controls the voltage between the source and the drain. If the negative voltage applied to the gate is high enough, it can remove all the electrons from the gate and thus close the conducting channel in which the electrons flow. Thus, the FET gets blocked.

¹ $\text{YBa}_2\text{Cu}_3\text{O}_{7-\delta}$ [43], $\text{YBa}_2\text{Cu}_4\text{O}_8$ [44], $\text{Bi}_2\text{Sr}_2\text{CaCu}_2\text{O}_8$ [45–47], $\text{Bi}_2\text{Sr}_2\text{CuO}_6$ [48], the infinite-layered superconductor $\text{Sr}_{1-x}\text{Ca}_x\text{CuO}_2$ [49], $\text{HgBa}_2\text{Ca}_2\text{Cu}_3\text{O}_{8+\delta}$ [50], $\text{HgBa}_2\text{CuO}_{4+\delta}$ [51], $\text{HgBa}_2\text{Ca}_{n-1}\text{Cu}_n\text{O}_{2n+2+\delta}$ [52], $\text{Tl}_2\text{Ba}_2\text{Ca}_{n-1}\text{Cu}_n\text{O}_{4+2n}$, [9], $\text{Sr}_2\text{CuO}_2\text{F}_2$, $\text{Sr}_2\text{CuO}_2\text{Cl}_2$, $\text{Ca}_2\text{CuO}_2\text{Cl}_2$ [53].

The system, considered in this section is in hydrodynamic regime, which means low frequency regime where the temperature of the superconducting film adiabatically follows the dissipated Ohmic power. All working frequencies of the lock-in's, say up to 100 kHz, are actually low enough. The investigations of superconducting bolometers show that only in the MHz range it is necessary to take into account the specific heat of the superconducting film. As an example there is a publication, corresponding to this topic [63]. In Ref. [64] we have proposed an experiment with a FET, for which we need to measure the second harmonic of the source-gate voltage and the third harmonic of the source-drain voltage. Other higher harmonics will be present in the measurements (e.g., from the leads), but in principle they can also be used for determining the DOS. An analogous experimental research has already been performed for investigation of thermal interface resistance [65]. The suggested experiment can be conducted using practically the same experimental setup, only the gate electrodes should be added to the protected by insulator layer superconducting films.

Here we suggest a simple electronic experiment to determine the logarithmic derivative of the density of states by electronic measurements using a thin film of $\text{Tl}_2\text{Ba}_2\text{CuO}_{6+\delta}$. The thickness of the samples should be typical for the investigation of high- T_c films, say 50–200 nm. Such films demonstrate already the properties of the bulk phase. The numerical value of this parameter

$$\nu'(E_F) = \left. \frac{d\nu(\epsilon)}{d\epsilon} \right|_{\epsilon=E_F}, \quad (1.23)$$

will ensure the absolute determination of hopping integrals.

We propose a field effect transistor (FET) of $\text{Tl}_2\text{Ba}_2\text{CuO}_{6+\delta}$ Fig. 1.7 to be investigated electronically with lock-in at second and third harmonics. Imagine a strip of $\text{Tl}_2\text{Ba}_2\text{CuO}_{6+\delta}$ and between the ends of the strip, i.e., between the source (S) and the drain (D) is applied an AC current

$$I_{SD}(t) = I_0 \cos(\omega t). \quad (1.24)$$

For low enough frequencies the ohmic power P increases the temperature of the film T above the ambient temperature T_0

$$P = RI_{SD}^2 = \alpha(T - T_0), \quad (1.25)$$

where the constant α determines the boundary thermo-resistance between the $\text{Tl}_2\text{Ba}_2\text{CuO}_{6+\delta}$ film and the substrate, and $R(T)$ is the temperature dependent source-drain (SD) resistance. We suppose that for thin film the

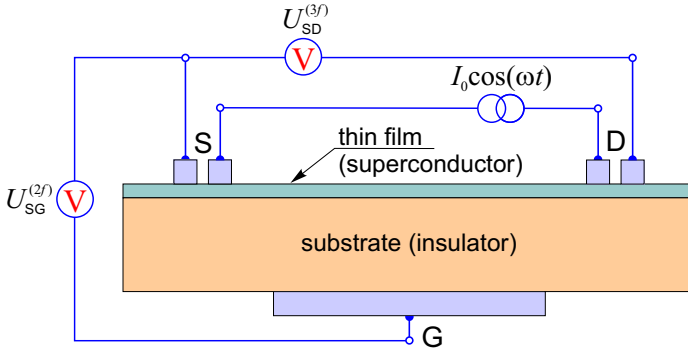


Fig. 1.7 A field effect transistor (FET) is schematically illustrated. The current $I(t)$, applied between the source (S) and the drain (D) has frequency ω . Running through the transistor the electrons create voltage U_{SG} with double frequency 2ω between the source (S) and the gate (G). The source-drain voltage U_{SD} is measured on the triple frequency 3ω .

temperature is almost homogeneous across the thickness of the film. In such a way we obtain for the temperature oscillations

$$T - T_0 = \frac{R I_{SD}^2}{\alpha} = \frac{R I_0^2}{\alpha} \cos^2(\omega t). \tag{1.26}$$

As the resistance is weakly temperature dependent

$$R(T) = R_0 + (T - T_0)R'_0, \quad R'_0(T_0) = \left. \frac{dR(T)}{dT} \right|_{T_0}. \tag{1.27}$$

A substitution here of the temperature oscillations from Eq. (1.26) gives a small time variations of the resistance

$$R(t) = R_0 \left(1 + \frac{R'_0}{\alpha} I_0^2 \cos^2(\omega t) \right). \tag{1.28}$$

Now we can calculate the source-drain voltage as

$$U_{SD}(t) = R(t)I_{SD}(t). \tag{1.29}$$

Substituting here the SD current from Eq. (1.24) and the SD resistance from Eq. (1.28) gives for the SD voltage

$$U_{SD}(t) = U_{SD}^{(1f)} \cos(\omega t) + U_{SD}^{(3f)} \cos(3\omega t). \tag{1.30}$$

The coefficient in front of the first harmonic $U_{SD}^{(1f)} \approx R_0 I_0$ is determined by the SD resistance R_0 at low currents I_0 , while for the third harmonic signal using the elementary formula $\cos^3(\omega t) = (3 \cos(\omega t) + \cos(3\omega t))/4$ we obtain

$$U_{SD}^{(3f)} = \frac{U_{SD}^{(1f)}}{4\alpha} I_0^2 R'_0. \tag{1.31}$$

From this formula we can express the boundary thermo-resistance by electronic measurements

$$\alpha = \frac{U_{SD}^{(1f)}}{4U_{SD}^{(3f)}} I_0^2 R_0'. \quad (1.32)$$

The realization of the method requires fitting of $R(T)$ and numerical differentiation at working temperature T_0 ; the linear regression is probably the simplest method if we need to know only one point.

Given α , we can express the time oscillations of the temperature substituting in Eq. (1.26)

$$T = T_0 + \frac{R I_0^2}{2\alpha} [1 + \cos(2\omega t)] \approx T_0 \left(1 + \frac{R_{SD} I_0^2}{2\alpha T_0} \cos(2\omega t) \right). \quad (1.33)$$

In this approximation terms containing I_0^4 are neglected and also we consider that shift of the average temperature of the film is small.

The variations of the temperature lead to variation of the work function of the film according to the well-known formula from the physics of metals

$$W(T) = -\frac{\pi^2}{6e} \frac{\nu'}{\nu} k_B^2 T^2, \quad \nu'(E_F) = \left. \frac{d\nu}{d\epsilon} \right|_{E_F}, \quad (1.34)$$

where the logarithmic derivative of the density of states $\nu(\epsilon)$ taken for the Fermi energy E_F has dimension of inverse energy, the work function W has dimension of voltage, T is the temperature in °K and k_B is the Boltzmann constant. For an introduction see the standard text books on statistical physics and physics of metals. [66, 67] Substituting here the temperature variations from Eq. (1.33) gives

$$W = -\frac{\pi^2 k_B^2}{6e} \frac{\nu'}{\nu} T_0^2 \left[1 + \frac{R_0 I_0^2}{\alpha T_0} \cos(2\omega t) \right] + O(I_0^4), \quad (1.35)$$

where \mathcal{O} -function again marks that the terms having I_0^4 are negligible.

The oscillations of the temperature creates AC oscillations of the source-gate (SG) voltage. We suppose that a lock-in with a preamplifier, having high enough internal resistance is switched between the source and the gate. In these conditions the second harmonics of the work function and of the SG voltage are equal

$$U_{SG}^{(2f)} = -\frac{\pi^2 k_B^2}{6e} \frac{\nu'}{\nu} T_0^2 \frac{R_0 I_0^2}{\alpha T_0}, \quad (1.36)$$

$$U_{SG}(t) = U_{SG}^{(2f)} \cos(2\omega t) + U_{SG}^{(4f)} \cos(4\omega t) + \dots \quad (1.37)$$

Substituting α from Eq. (1.32) we have

$$U_{\text{SG}}^{(2f)} = -\frac{4\pi^2 k_{\text{B}}^2}{6e} \frac{\nu'}{\nu} \frac{U_{\text{SD}}^{(3f)} T_0}{I_0 R_0'}. \quad (1.38)$$

From this equation we can finally express the pursued logarithmic derivative of the density of states

$$\left. \frac{d \ln \nu(\epsilon)}{d\epsilon} \right|_{E_{\text{F}}} = \frac{\nu'}{\nu} = -\frac{3e}{2\pi^2 k_{\text{B}}^2} \frac{I_0}{T_0} \frac{U_{\text{SG}}^{(2f)}}{U_{\text{SD}}^{(3f)}} \frac{dR}{dT}. \quad (1.39)$$

In such way the logarithmic derivative of the density of states can be determined by fully electronic measurements with a FET. This important energy parameter can be used for absolute determination of the hopping integrals in the generic LCAO model. The realization of the experiment can be considered as continuation of already published detail theoretical and experimental investigations and having a set of complementary studies we can reliably determine the LCAO parameters.

We predict largest DOS logarithmic derivative values, associated with a sign change as well, for $\text{La}_{2-x}\text{Sr}_x\text{CuO}_4$, $0.09 < x < 0.22$, as the Fermi contour topology changes, see Fig. 3.44 in Ref. [2] and Refs. [68–71].